3.3.2. Comparison of $RuFe/SiO_2$ and Ru/SiO_2

Run 4 has been carried out with Ru/SiO_2 which contained as much ruthenium as the 5.5 wt% $RuFe(1:3)/SiO_2$ catalyst that was used in run 3. The aim of this run was to investigate the effect of the addition of iron to ruthenium supported on silica on the activity and selectivity.

A fresh Ru/SiO_2 catalyst deactivates rapidly and similarly as $RuFe/SiO_2$, as shown in Figure 3.4. It is interesting to note that initially the catalyst is very active while it produces a great deal of water, resulting in a high water vapour pressure. This is shown by the first data point in Table 3.4 (experiment 1.1). As will demonstrated later, water strongly inhibits the reaction which means that even higher activities should be expected if measurements were made at a lower conversion level.

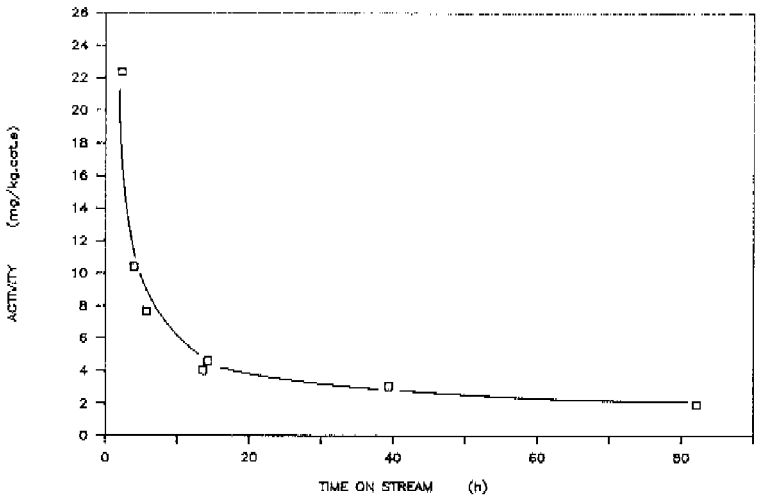

Fig. 3.4 The activity of a fresh Ru/SiO_2 catalyst as a function of time on stream (see experiments 1-4 of Table 4)

It appears that the activity of Ru/SiO_2, after the steady-state is reached, is hardly different from the activity of $RuFe/SiO_2$ as demonstrated in Table 3.6. It can thus be concluded that the addition of iron to Ru supported on silica hardly influences the steady-state activity reached after a moderate time on stream.

Table 3.6

The activity of 2.1 wt% Ru/SiO_2 and 5 wt% $RuFe/SiO_2$ at 9 bar and 250°C.

Catalyst	Run no.	H.O.S.	P_{H_2} [bar]	P_{CO} [bar]	F_{in} [ml/min] [1]	Activity [2]
5.0 wt%(1:3)$RuFe/SiO_2$	2	238	5.96	2.62	228	1.4
5.5 wt%(1:3)$RuFe/SiO_2$	3	116	5.80	2.55	214	1.6
2.1 wt%Ru/SiO_2	4	215	5.67	3.20	208	1.1

[1] measured at 20°C and 1 bar

[2] [mg C_1–C_7/kg cat.s]

3.3.3 Comparison of $RuFe/SiO_2$, Ru/SiO_2 and fused iron

Comparison of $Ru(Fe)/SiO_2$ and fused iron catalysts promoted with potassium (see 2.2) shows remarkable differences. The activity of fused iron is not only much higher at comparable reaction conditions but the increase of the activity versus the temperature is also larger for fused iron as is clearly shown in Figure 3.5. It has to be noted that the activities in Figure 3.5 are related to the total weight of the catalyst (including support material). This means that the activity differences are less pronounced when only considering the weight of the metals. No reliable data is available to compare the catalyst on the basis of the metal surface exposed.

3.3.4 Kinetic model for $RuFe/SiO_2$

The influence of the total pressure, the H_2 pressure, the CO pressure and the water vapour pressure on the activity and conversion of synthesis gas over $RuFe/SiO_2$ resulting in an emperical kinetic relation will be presented in this section. The results are based on the experiments carried out during run 3.

Regarding the performance of $RuFe/SiO_2$ at higher pressures, the influence of the total pressure on the conversion of CO over fused iron was investigated first. As demonstrated in Chapter 2, the conversion of synthesis gas over fused iron is linearly proportional to the hydrogen pressure up to a high conversion. Increasing the total pressure therefore, results in an increase of the conversion of CO as shown in

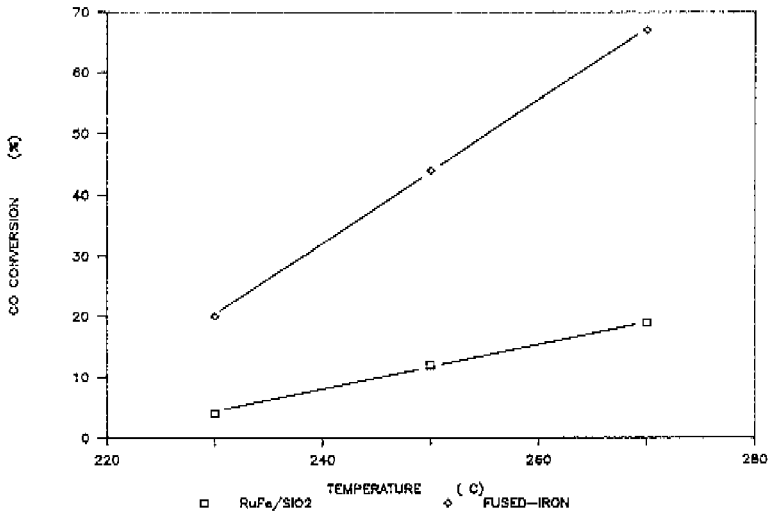

Fig. 3.5 The conversion of CO as a function of temperature for both $RuFe/SiO_2$ and potassium promoted fused iron. Reaction conditions: pressure = 9 bar; H_2/CO ratio = 1; gas flow in = 200 ml (20°C, 1 bar)/min

Table 3.7. Surprisingly, the pressure does not significantly affect the conversion of CO over $RuFe/SiO_2$ despite an increase of the H_2 pressure with a factor 10 as shown in Table 3.8. Apparently, the conversion of synthesis gas is strongly hampered. The effect of the H_2 pressure has been investigated by keeping the pressure of CO constant. As expected, the pressure of H_2 has a positive effect on the activity of $RuFe/SiO_2$ as shown in Table 9. However, the precise relation between the pressure of H_2 and the activity is not very clear and complicated by the fact that the increasing water vapour pressure interferes (see below).

Table 3.7

The effect of the pressure on the conversion of CO over fused iron (C73) at 250°C. The H_2/CO inlet ratio was 0.67

Flow [ml/min] [1]	H_2/CO [-]	P_{H_2} [bar]	P [bar]	X_{CO} [%]
287	0.70	0.5	1.2	5
291	0.80	3.2	9.0	44
298	0.94	5.7	17.0	64

[1] measured at 20°C and 1 bar

Table 3.8

The effect of the pressure on the conversion of CO over $RuFe/SiO_2$ at 250°C. The H_2/CO ratio was approximately constant (run 3)

Experiment number	Flow [ml/min] [1]	H_2/CO [-]	X_{CO} [%]	P [bar]	P_{H_2} [bar]
21	235	2.4	11	1.4	0.9
6	209	2.2	16	9.0	5.8
11	207	2.1	14	17.0	10.8

[1] measured at 20°C and 1 bar

Contrary to this effect of H_2, CO inhibits the conversion of synthesis gas. The activity obviously decreases with increasing pressure of CO as shown in Figure 3.6.

The effect of the water vapour pressure has been investigated by the addition of a water-gas shift catalyst which provides for the conversion of product water into CO_2 until the watergas-shift equilibrium is reached. Both the conversion of CO and H_2 as well as the activity increase, and a rather large portion is converted to CO_2, as shown in Table 3.10. The increase of the activity can be attributed almost completely to the decrease of the water vapour pressure because the pressure of H_2 does not change while the decrease of the CO pressure has but a small effect as shown in Figure 3.6. This experimental proof of the inhibition by water can be used to explain the moderate effect of the

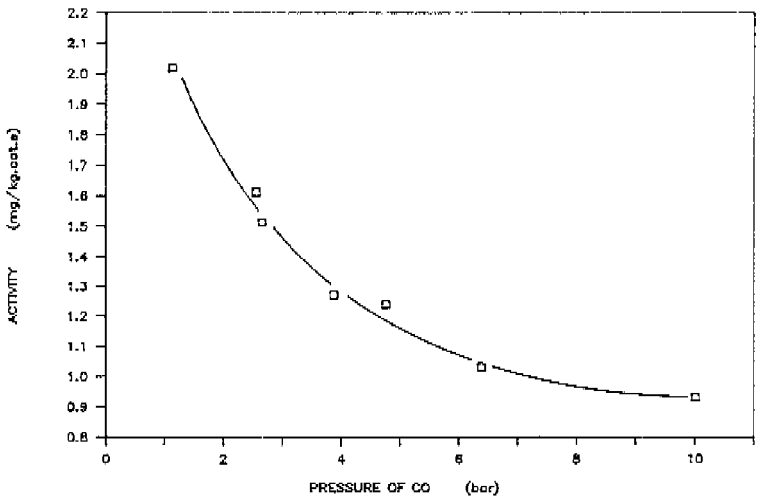

Fig. 3.6 The influence of the CO pressure on the activity of RuFe/SiO_2 (run 3, experiment 3-10). The H_2 pressure was approximately 5.7 bar

increase of H_2 on the activity as shown in Table 3.9. It is clear that the increase of the H_2 pressure results in a higher H_2O pressure due to a higher conversion level. This increased water vapour pressure causes a decrease of the activity which is only slightly smaller than the increase by H_2, resulting in an irregular activity pattern with increasing H_2 pressure as shown in Table 3.9.

Table 3.9

The influence of the H_2 pressure on the activity of $RuFe/SiO_2$ (run 3). Other reaction conditions are reported in Table 3.3

Exp. no.	P_{H_2} [bar]	P_{CO} [bar]	P_{H_2O} [bar]	Activity [mg/kg.cat.s]
15	1.8	5.0	0.059	0.84
13	2.9	4.9	0.063	0.78
17	3.3	5.0	0.13	1.46
16	3.8	5.1	0.15	1.62
14	5.1	4.9	0.15	1.40
12	7.5	4.9	0.18	1.36
11	10.8	5.0	0.31	1.79

Before attempting to express the effect of the partial pressure of H_2, CO and H_2O in a kinetic model, some relations proposed in literature will be discussed.

A prerequisite for the model to be selected is a negative influence of both the pressure of CO and H_2O on the conversion rate of synthesis gas. Keeping this in mind, the relation proposed by Huff and Satterfield [16] must be rejected. Although this relation does account for the decrease of the reaction rate at a higher degree of conversion over a fused iron catalyst, it does not describe inhibition at increasing CO pressure:

$$-r_{CO+H_2} = \frac{a\ P_{H_2}\ P_{CO}\ P_{H_2}/P_{H_2O}}{1 + b\ P_{CO}\ P_{H_2}/P_{H_2O}} \qquad (3.1)$$

The kinetic relation of Anderson [17] and Dry [18] based on the CO insertion theory can also be ruled out because this relation assumes that CO and H_2O compete for the same active sites:

$$-r_{CO+H_2} = \frac{a\ P_{H_2}}{1 + b\ P_{H_2O}/P_{CO}} \qquad (3.2)$$

The pressure of CO actually has a positive effect on the rate in this relation which is certainly not the case for this catalyst as earlier shown in Figure 3.6.

Table 3.10

The effect of a decrease of the water vapour pressure on the activity of $RuFe/SiO_2$. The water vapour pressure was lowered by the addition of a water-gas shift catalyst (run 3)

Exp. no.	P_{H_2O} [bar]	P_{CO_2} [bar]	P_{H_2} [bar]	P_{CO} [bar]	X_{CO} [3)] [%]	X_{H_2} [%]	Activity [mg/kg.cat.s]
26	0.13 [1)]	<0.005	6.3	2.5	8.6	13.3	3.19
27	0.02 [2)]	0.48	6.2	1.8	15.1	18.6	5.48

1) calculated from hydrocarbons produced

2) calculated by means of the water-gas shift equilibrium

3) based on the conversion to hydrocarbons

Dixit and Taviarides [19] proposed a model based on kinetic data obtained on 0.5% Ru/Al_2O_3 at a high degree of conversion and pressures up to 10 bar, at steady state conditions (which are hardly available for supported ruthenium catalysts):

$$-r_{CO} = \frac{a\ P_{CO}\ P_{H_2}}{(1 + b\ P_{CO})^2} \qquad (3.3)$$

This model is based on the assumption that the rate determining step is the hydrogenation of adsorbed CH_x species. This fits in with the kinetic data moderately well, because in this model inhibition by CO is accounted for. However, the data can be described better with a model that accounts for the adsorption of H_2O also.

As such model has not been presented in literature for RuFe catalysts, two models were developed in this study based on the reaction network proposed for supported Ruthenium by Kellner and Bell [20]. The latter has been adjusted because also Kellner and Bell do not account for water inhibition (see appendix 1)either. In the models developed the assumption is made that the rate determining step is the hydrogenation of adsorbed CH_x species. In model I the assumption is that surface oxygen reacts with hydrogen irreversibly in contrast with model II, wherein this reaction is assumed reversible. The best fit is obtained with model I, thereby assuming further that

* the rate determining step is the hydrogenation of θ_{CH}
* carbon and water saturate the active sites:

This results in the following simplified expression:

$$-r_{CO} = \frac{a\ P_{CO}^{1/2}\ P_{H_2}}{(P_{CO}^{1/2} + b\ P_{H_2O})^2} \qquad (3.4)$$

with a is 1.14 and b is 4.3.
The experimental data and the predicted rate of conversion of CO are shown in Figure 3.6 and 3.7. Eq.(3.4) shows the strong inhibition of CO and H_2O. It is clear that the activity of RuFe decreases sharply with decreasing space velocity due to the decrease of the H_2 pressure and the replacement of CO by H_2O which supresses the activity even more than CO, as demonstrated in Eq.(3.4).

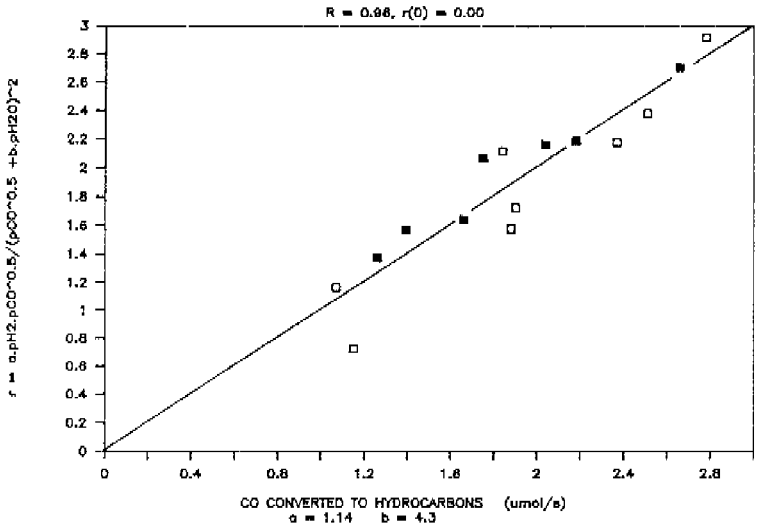

Fig. 3.7 Comparison of experimental and predicted rate of CO conversion for $RuFe/SiO_2$ (run 3, experiment 3-20). The closed symbols are the same experiments as shown in Figure 3.6

3.3.5. Kinetic model for Ru/SiO_2

A single run with Ru/SiO_2 has been carried out to compare the kinetics over Ru/SiO_2 and $RuFe/SiO_2$. A reliable critical assessment of models for the kinetics over Ru/SiO_2 is not possible in view of the limited number of experiments. However, the data can be used to obtain an indication of the similarity between the kinetics of both catalysts. The experimental data is well described by Eq.(3.4) which has been derived for $RuFe/SiO_2$; only the parameters a and b are somewhat different:

$$-r_{CO} = \frac{0.58\ P_{H_2}\ P_{CO}^{\frac{1}{2}}}{(P_{CO}^{\frac{1}{2}} + 10 P_{H_2O})^2} \qquad (3.5)$$

It is interesting to note that the rather close correspondence between the kinetics for $RuFe/SiO_2$ and Ru/SiO_2 indicates that the presence of Ru dominates the performance of these catalysts.

3.3.6 Product distribution over $RuFe/SiO_2$

This section starts with the description of the product distribution of a fresh catalyst, followed by that of a used catalyst at various temperatures and pressures and ends with some remarks on the Schulz-Flory distribution.

During the first hours on stream, traces of CO_2 were observed but the CO_2 production fell sharply to such low level that it was not measurable during all other experiments. This indicates that the rate of the water-gas shift reaction is rather low with respect to the production and removal of water from the reactor.

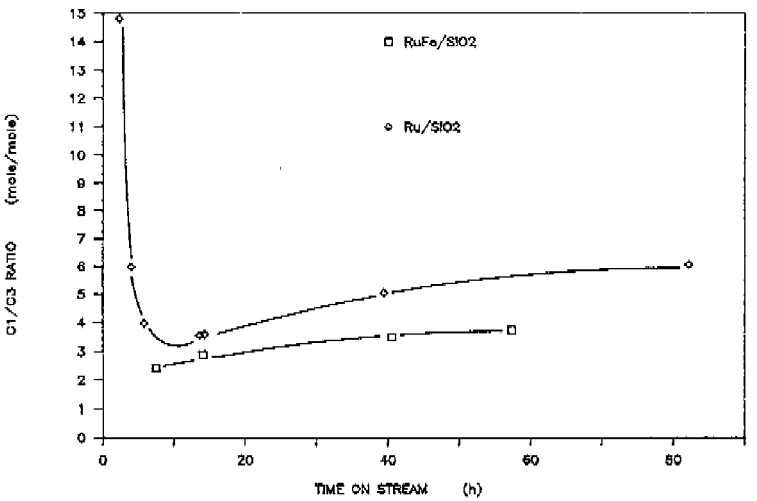

Fig. 3.8 The C_1/C_3 mole ratio as a function of time on stream for both $RuFe/SiO_2$ and Ru/SiO_2 (run 3 and 4, respectively)

During this initial period the product distribution changes in spite of the low reactor temperature. Figure 3.8 shows that the C_1/C_3 ratio increases gradually during the first 60 hours on stream at 230°C, indicating that the value of α decreases during this period.

During run 1 and run 2 the temperature was increased with increasing time on stream which caused a decrease of the value of α (see Figure 3.9 and 3.10). This decline of α is irreversible. Figure 3.9 shows that when the temperature is reduced from 280 to 250°C, α does not significantly change. After the temperature reduction to 250°C, the value of α versus time on stream is constant also, as shown in Figure 3.10 (see experiment number 10 and 13). When, however, the temperature is increased again to a higher level, the value of α at 250°C is lower than before this rise of temperature took place (compare no. 13 and 16 in Figure 3.10). This means that a second temporary temperature increase may again result in a lower α. Summarizing, the value of α decreases irreversibly and slowly at a low

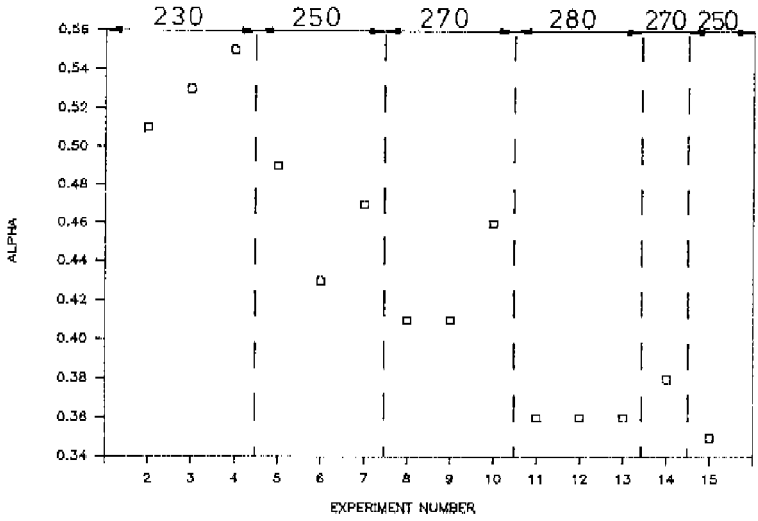

Fig. 3.9 Summary of the values of α of Rufe/SiO_2 for all experiments of run 1. The temperature is reported on the upper side

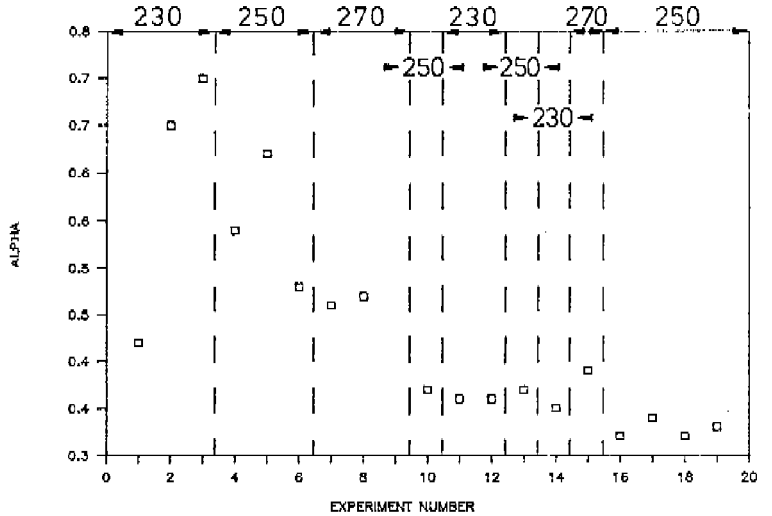

Fig. 3.10 Summary of the values of α of $RuFe/SiO_2$ for all experiments of run 2. The temperature is reported on the upper side

constant temperature to a steady-state value (as shown for a fresh catalyst in Figure 3.8). This decline is enhanced by a higher temperature.

This knowledge is applied to run 3. The temperature at the beginning of this run was kept constant at a relatively high temperature level (280°C) until the steady-state was reached (this steady-state was desired for kinetic experiments). Figure 3.11 demonstrates that α stayed almost constant after this "high temperature treatment" during the experiments 2-20, which cover a time period of 700 hours on stream. It is noteworthy that the behaviour of α versus time on stream corresponds with that of the activity. Thus, if the value of α is constant or decreases, the activity keeps constant or decreases as well.

The influence of the pressure on α is shown in Figure 3.11. The mean value of α is obviously lower for low pressure experiments (no. 21-25.4)

than for experiments at higher pressure (no. 2-20). Although the value of α increases with increasing pressure, it appears that the C_1/C_3 ratio hardly depends on the pressure as shown in Table 3.11. In fact, the methane fraction exceeds the value predicted by the Schulz-Flory distribution at high pressures (see Figure 3.12).

In contrast to the C_1/C_3 ratio, the C_1/C_2 ratio increases with increasing pressure due to the decrease of the C_2 fraction, probably caused by insertion of ethene (see Table 3.11). This ethene insertion may thus be responsible for the dip in the Schulz-Flory distribution at carbon number 2, as clearly shown in Figure 3.12.

Table 3.11

The influence of the pressure on the product distribution of $RuFe/SiO_2$ at an approximately constant H_2/CO ratio (run 3)

Experiment number	H.O.S. [h]	H_2/CO [mol/mol]	Pressure [bar]	C_1/C_1-C_4 [mol/mol]	C_1/C_2 [mol/mol]	C_1/C_3 [mol/mol]
25	904	2.5	1.4	73	5	8
21	784	2.4	1.4	73	5	8
22	793	2.4	1.4	74	5	8
6	256	2.2	9.0	76	9	7
3	135	2.3	9.0	79	9	9
11	423	2.1	17.0	79	11	9

3.3.7 Product distribution over Ru/SiO_2 and comparison with $RuFe/SiO_2$

The outlet gas of the reactor freshly charged with Ru/SiO_2 and running for two hours at 250°C and 9 bar, consists almost exclusively of methane. The C_1/C_3 ratio decreases sharply with increasing time on stream as shown in Figure 3.11. This is due to the strong decrease of the methane production rate which is expressed by the activity decrease (Figure 3.4). However, the methane fraction and the C_1/C_3 ratio reach a minimum and start to increase again after approximately 10 hours on stream. This increase is similar to that of $RuFe/SiO_2$. The increase of

the C_1/C_3 ratio flattens after 60 hours on stream. After this point of time the C_1/C_3 ratio remained practically constant.

The product distribution for Ru/SiO_2 has been investigated for various H_2/CO ratios. Both the methane and the C_1/C_3 ratio decrease with increasing H_2/CO ratio, as generally reported. More important is the remarkable similarity of the methane fraction and the C_1/C_3 ratio for $RuFe/SiO_2$ and Ru/SiO_2, as shown in Table 3.12. Thus, the product distributions of both catalysts appear to resemble each other closely.

In accordance with $RuFe/SiO_2$, the C_2 fraction for Ru/SiO_2 also shows a considerable dip in the Schulz-Flory distribution as shown in Figure 3.13. The C_2 fraction was even lower than the C_3 fraction for all experiments. Assuming that the deviation of the C_2 fraction is caused by

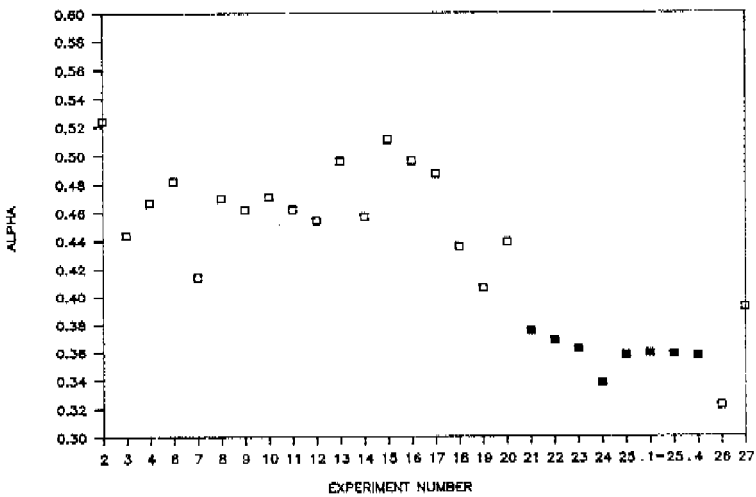

Fig. 3.11 Summary of the values of α of $RuFe/SiO_2$ for all experiments of run 3. Open symbols: high pressure; filled symbols: low pressure

the insertion of ethene in the chain growth this indicates that this secondary reaction of ethene occurs very rapidly over both catalysts despite the very low CO conversion and ethene concentration.

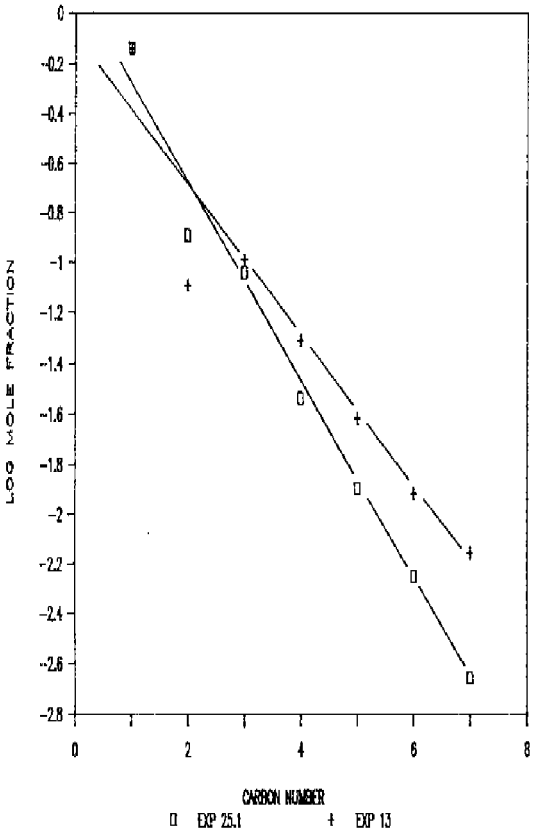

Fig. 3.12 Schulz-Flory distribution for RuFe/SiO_2 (run 3) at a low pressure (experiment 25.1) and a high pressure (experiment 13). The reaction conditions are reported in Table 3.3

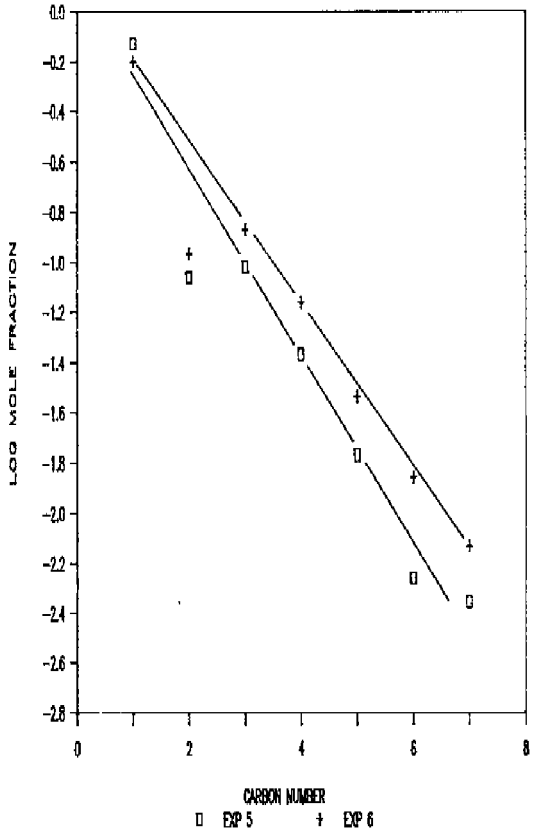

Fig. 3.13 Schulz-Flory distribution for Ru/SiO_2 (run 4) at a low and high H_2/CO ratio (experiment 5 and 6 respectively). The reaction conditions are reported in Table 3.3

Table 3.12

The effect of the H_2/CO ratio on the product distribution for both $RuFe/SiO_2$ (run 3) and Ru/SiO_2 (run 4) at 250°C

Experiment number		H.O.S.		H_2/CO [mol/mol]	Pressure [bar]		C_1/C_3 ratio [mol/mol]		C_1 fraction [mol %]	
RuFe	Ru	RuFe	Ru		RuFe	Ru	RuFe	Ru	RuFe	Ru
11	-	423	-	2.1	17	-	8.6	-	76.7	-
12	-	447	-	1.5	13	-	8.8	-	76.4	-
14	5	496	307	1.1	10.5	10.6	7.9	7.8	74.8	74.4
16	-	592	-	0.8	9.0	-	6.4	-	70.5	-
17	8	616	370	0.7	8.5	8.5	5.9	6.2	68.0	69.5
15	-	531	395	0.4	6.8	7.0	5.5	4.6	66.5	62.5

3.3.8 Olefin selectivity for $RuFe/SiO_2$

In this section the dependence of the olefin selectivity on the reaction conditions and the time on stream of $RuFe/SiO_2$ is considered.

After some notes on the olefin selectivity of a fresh catalyst, the influence of the process conditions on the olefin selectivity will be discussed. The course of the C_2 and C_3 olefin selectivity as a function of time on stream for a fresh $RuFe/SiO_2$ catalyst (the start of run 2) is shown in Figure 3.14. The magnitude of the olefin selectivity is surprisingly low in view of results at low pressure [3], the low conversion of CO (< 10%) and the low temperature (230°C). The increase of the olefin selectivity with increasing time on stream is mainly caused by the decline of CO conversion which is also shown in Figure 3.14. The low olefin selectivity after only a few hours on stream shows that the hydrogenation of olefins occurs very rapidly over fresh $RuFe/SiO_2$ at a high pressure (9 bar) and under conditions which are certainly not differential.

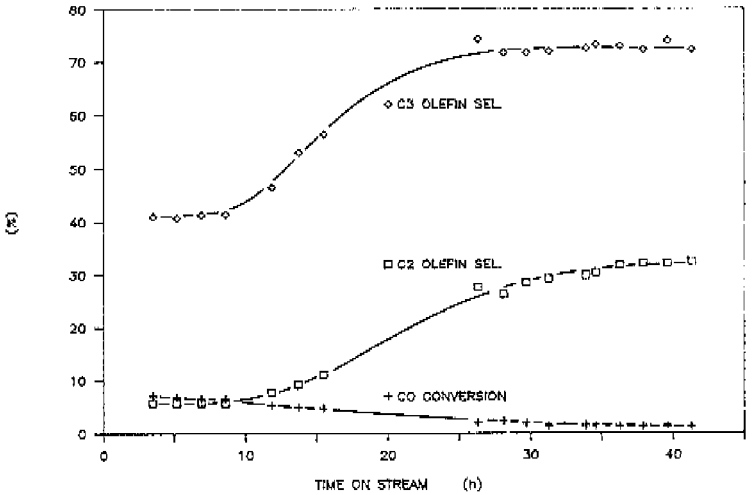

Fig. 3.14 The C_2 and C_3 olefin selectivity and CO conversion as a function of time on stream for a fresh $RuFe/SiO_2$ catalyst (run 2) The CO conversion shown is based on CO converted in C_1-C_3 hydrocarbons. The reaction conditions are reported in Table 3.2

The effect of changing of reaction temperature on the olefin selectivity has been investigated for three H_2/CO ratios. At the highest H_2/CO ratio the olefin selectivity of C_2, C_3 and C_4 apparently decreases with increasing temperature as shown in Figure 3.15. At a lower H_2/CO ratio, however, the C_3 and C_4 olefin selectivity increase with increasing temperature despite the increase of both the conversion of CO and the pressure of olefins. This increase of the olefin selectivity may be caused by a decrease of the formation of paraffins directly from synthesis gas. A decrease of the secondary hydrogenation rate with respect to the Fischer-Tropsch synthesis rate, which would also explain the olefin selectivity increase, is unlikely in view of the small temperature dependence of the Fischer-Tropsch synthesis (see Figure 3.5).

The effect of the H_2/CO ratio is shown in Figure 3.15. This figure demonstrates that the olefin selectivity increases when the H_2/CO ratio is lowered. It has to be noted that this increase of the olefin selectivity can be caused both by the lower H_2/CO ratio as such and by the decreased CO conversion level. The effect of the pressure of H_2 and CO on the olefin selectivity will be shown later.

As pointed out in section 2.11, the olefin selectivity will increase with increasing carbon number when the value of α is lower than 0.6. This is due to the fact that at α below 0.6 the concentration of hydrocarbons decreases with increasing carbon number, in spite of a decreasing volatility. In accordance with this prediction, the C_4 olefin selectivity is indeed always higher than the C_3 olefin selectivity (see Figure 3.15).

The influence of the pressure of both CO and H_2 has been investigated by varying the CO pressure at a constant H_2 pressure and reverse, in order to verify the competition model, presented in section 2.9 for fused iron, for the results of $RuFe/SiO_2$. The effect of the CO pressure will

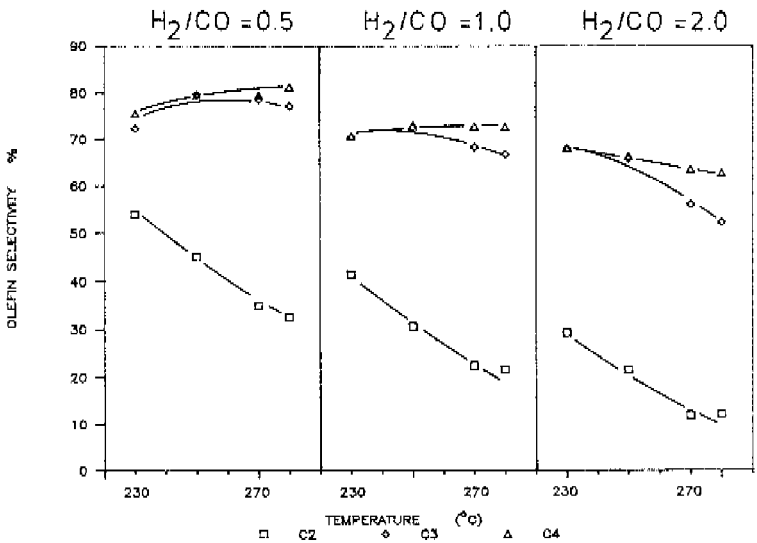

Fig. 3.15 The olefin selectivity for $RuFe/SiO_2$ as a function of the temperature at various H_2/CO ratios (run 1)

first be considered, followed by that of the H_2 pressure.

When the pressure of H_2 is kept constant, the C_2 and C_3 olefin selectivity increases with increasing CO pressure as shown in Figure 3.16. This increase of the olefin selectivity correlates with a decline of the olefin/CO pressure ratio alone, as shown by the data reported in Figure 3.16.

Unfortunately, this correlation is no longer valid when the H_2 pressure is varied over a large range. The decline of the olefin selectivity cannot be explained by a change of the olefin/CO pressure ratio alone as shown in Figure 3.17. Although the olefin/CO pressure ratio for the first two data points increases, this ratio does not significantly change further in respect of the other data points whereas the olefin selectivity continues to decrease. Apparently, the increase of the H_2 pressure promotes the formation of paraffins. It is not clear from

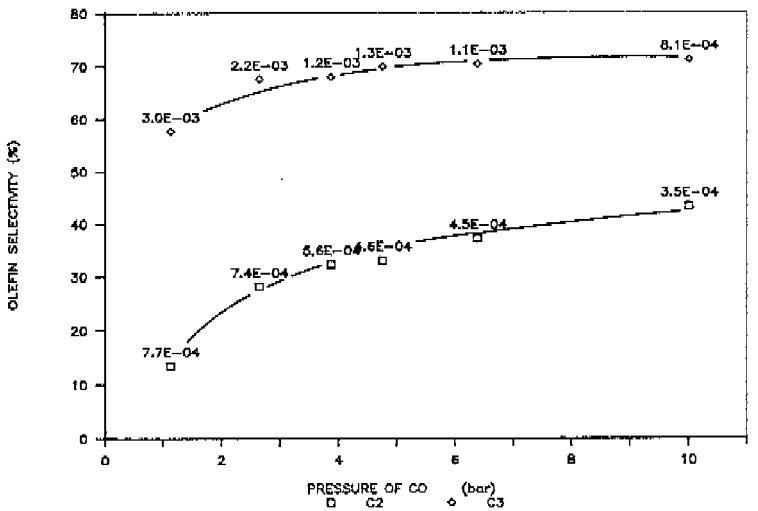

Fig. 3.16 The C_2 and C_3 olefin selectivity for $RuFe/SiO_2$ as a function of the CO pressure (run 3). The H_2 pressure is approximately 5.7 bar. The numbers reported are the values of the olefin/CO pressure ratio

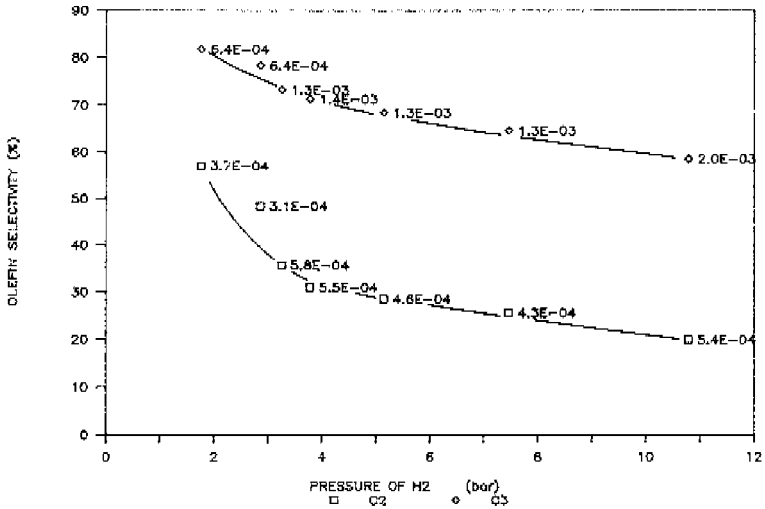

Fig. 3.17 The C_2 and C_3 olefin selectivity for $RuFe/SiO_2$ as a function of the H_2 pressure (run 3). The pressure of CO is approximately 5.0 bar. The numbers reported are the values of the olefin/CO pressure ratio

these experiments whether promotion of the primary formation of paraffins or enhancement of the secondary hydrogenation of olefins to paraffins is the main cause of the hydrogen influence. Note that when the secondary hydrogenation advances by a high H_2 pressure this may indicate that the overall order in hydrogen for this hydrogenation reaction is higher than that of the Fischer-Tropsch reaction. The influence of the H_2 pressure on the olefin selectivity implies that the parameter P_{olefin}/P_{CO} has to be modified to obtain a suitable parameter which correlates all experiments. The best fit is obtained when the data are correlated with the parameter $P_{olefin}P_{H_2}/P_{CO}^{1.4}$. This empirical parameter satisfactory describes the experimental data of both the C_2 and C_3 olefin selectivity in view of the large range of reaction conditions (1-17 bar, H_2/CO = 0.4-10) as shown in Figure 3.18 and 3.19.

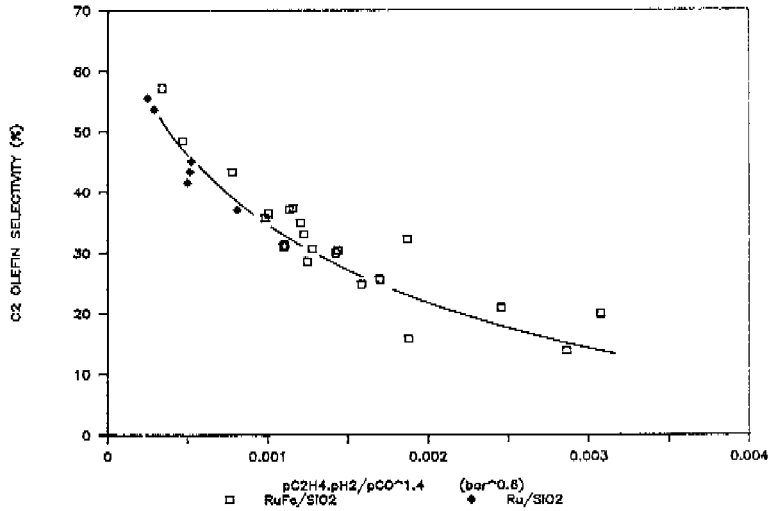

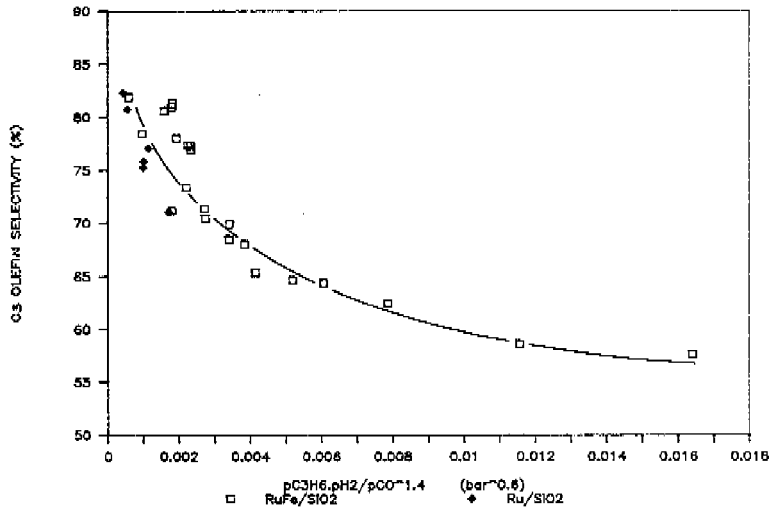

Fig. 3.18 and 3.19 The course of the olefin selectivity as a function of $P_{Olefin}P_{H_2}/P_{CO}^{1.4}$ *for both* $RuFe/SiO_2$ *(run 3) and* Ru/SiO_2 *(run 4)*

3.3.9 Olefin selectivity for Ru/SiO_2

In this section the olefin selectivity of Ru/SiO_2 will be handled. Firstly, the olefin selectivity of a fresh catalyst will be discussed. Secondly, the steady-state olefin selectivity will be considered and compared with that of $RuFe/SiO_2$.

The secondary hydrogenation as well as the Fischer-Tropsch activity of a fresh Ru/SiO_2 catalyst is very high. These properties of a fresh catalyst result in an extremely low olefin selectivity and in a high conversion of CO shortly after the start of the exposure to synthesis gas as shown in Figure 3.20. The olefin selectivity increases sharply with increasing time on stream whereas the conversion of CO decreases strongly. It is important to note that this increase of the olefin

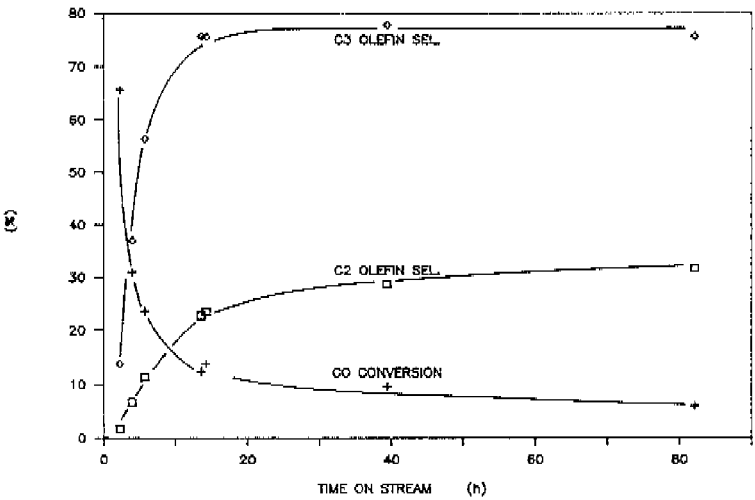

Fig. 3.20 The course of the olefin selectivity and CO conversion as a function of time on stream for a fresh Ru/SiO_2 catalyst (run 4). The CO conversion is based on CO converted to C_1-C_7 hydrocarbons

selectivity is not caused by the lower degree of CO conversion but is due to a strong decrease of the secondary hydrogenation. This is demontrated by the results in Table 3.13. It can be seen in this table that the partial pressures of the olefins increase initially and decline slowly later on, in contrast with the partial pressures of the C_2 and C_3 fractions which decrease sharply with increasing time on stream. Apparently, the decreased hydrogenation of olefins and a reduced formation of hydrocarbons by the Fischer-Tropsch reaction largely balance out.

Table 3.13

The olefin selectivity and the pressure of the C_2, C_3, C_2H_4 and C_2H_6 fractions as a function of time on stream for a fresh Ru/SiO_2 catalyst (run 4)

Exp. no.	H.O.S. [h]	pC_2H_4 [mbar]	pC_3H_6 [mbar]	pC_2 [mbar]	pC_3 [mbar]	Olefin selectivity (%) C_2	C_3
1.1	2.3	3.80	26.7	228.9	193.3	1.2	13.8
1.2	4.0	6.30	39.0	93.8	105.4	6.7	37.0
1.3	5.8	5.52	40.6	48.6	72.1	11.4	56.3
1.4	13.6	4.90	28.4	21.6	37.5	22.7	75.7
1.5	14.3	5.18	29.3	22.1	38.6	23.4	75.6
1.6	39.4	3.23	13.6	11.3	17.5	28.7	77.8
1.7	82.1	2.04	7.6	6.5	10.1	31.6	75.6

Another indication for the strong initial secondary hydrogenation is the C_2/C_3 mole ratio. The relatively high C_2 fraction which forms initially, as compared to the C_3 fraction indicates that the insertion of ethene does not occur due to the much more rapid hydrogenation to ethane. When the hydrogenation rate of ethene and other olefins (naturally also the Fischer-Tropsch activity) decreases with increasing time on stream, the insertion of ethene does occur, resulting in a decrease of the C_2 fraction with respect to the fraction of C_3.

The C_2 and C_3 olefin selectivity do not rise beyond 32 and 76% respectively after 40 hours on stream. The CO conversion declines to approximately 3% at the same time. These low values of the olefin selectivity at such a low conversion level means that the rate of the secondary hydrogenation of olefins over Ru/SiO_2 stays high with respect to the rate of the Fischer-Tropsch reaction.

The olefin selectivity of Ru/SiO_2 has been investigated at various reaction conditions after the steady-state activity was attained. The experimental data can be correlated with the same parameter as used for $RuFe/SiO_2$. Although it is not possible to conclude that this parameter is the optimum one to describe the dependence of the olefin selectivity on the reaction conditions, it fits the data points satisfactorily and gives an indication of the order of magnitude. Besides, the olefin selectivity can be compared in this way with the data obtained for $RuFe/SiO_2$. The Figures 3.18 and 3.19 clearly demonstrate that the C_2 and C_3 olefin selectivity for Ru/SiO_2 hardly differ from that of $RuFe/SiO_2$. Thus, not only activity and product distribution but also the magnitude of the olefin selectivity of $RuFe/SiO_2$ and Ru/SiO_2 are similar.

3.3.10 Comparison of the olefin selectivity over $RuFe/SiO_2$ and fused iron

In contrast with the small difference between the olefin selectivity of $RuFe/SiO_2$ and Ru/SiO_2, the degree of secondary hydrogenation of olefins between $RuFe/SiO_2$ and potassium promoted fused iron differ enormously. The C_3 olefin selectivity for both catalysts as a function of the optimum parameter for $RuFe/SiO_2$ is shown in Figure 3.21. As pointed out in Chapter 2 the p_{olefin}/p_{CO} ratio is the right parameter to describe the effect of the reaction conditions on the olefin selectivity for fused iron. Nevertheless for the purpose of merely giving an idea of the difference between the olefin selectivity of these two types of catalysts, the parameter $p_{C_3H_6}p_{H_2}/p_{CO}^{1.4}$ can be used also for fused iron if the pressures of H_2 and CO do not vary much. Obviously, the decline of the olefin selectivity is very severe for $RuFe/SiO_2$, with respect to the hardly noticable decrease of the C_3 olefin selectivity for fused iron over the range shown in Figure 3.21. The olefin selectivity of other hydrocarbon fractions demonstrates a similar pattern. A survey of the C_2 olefin selectivity for both catalysts at various reaction conditions is

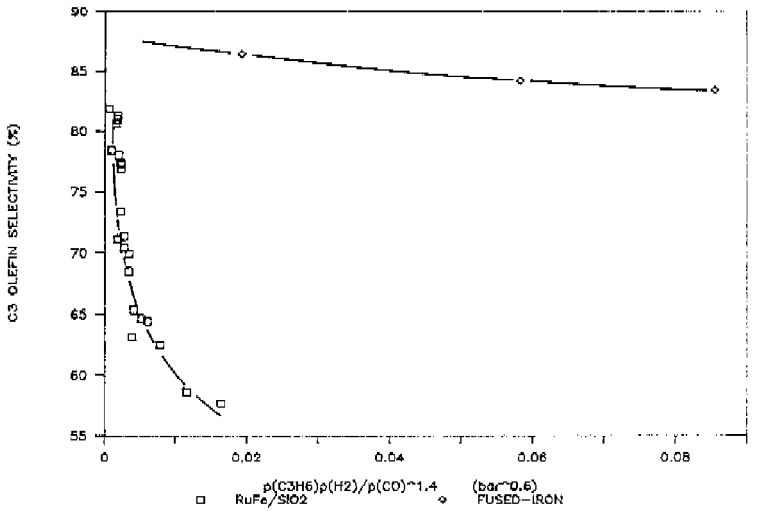

Fig. 3.21 Comparison of the C_3 olefin selectivity between $RuFe/SiO_2$ and potassium promoted fused iron at 250°C

presented in Table 3.14. This data clearly shows that the C_2 olefin selectivity for $RuFe/SiO_2$ is always lower than that of fused iron even at a low pressure and a low degree of CO conversion. The differences are extremely large at high pressure; particularly regarding the mole fraction of ethene with respect to the C_1-C_4 mole fraction (last column of Table 3.14). The final conclusion therefore is that the yield of olefins over $RuFe/SiO_2$ is much lower than that over potassium promoted fused iron because of a higher hydrogenation rate as well as a larger incorporation.